JPn Neuroscience

The Journal of Physiology

J Physiol 592.13 (2014) pp 2881–2897

Muscle-specific kinase (MuSK) autoantibodies suppress the MuSK pathway and ACh receptor retention at the mouse neuromuscular junction

Nazanin Ghazanfari[1], Marco Morsch[1], Stephen W. Reddel[2], Simon X. Liang[3] and William D. Phillips[1]

[1] *Physiology and Bosch Institute, University of Sydney, Sydney, New South Wales 2006, Australia*
[2] *Department of Molecular Medicine, Concord Hospital, Concord, New South Wales 2139, Australia*
[3] *Department of Biochemistry and Molecular Biology, College of Basic Medical Sciences, Liaoning Medical University, China*

Key points

- Myasthenic anti-muscle-specific-kinase (MuSK) IgG was injected into mice to study its effect upon the MuSK signalling pathway and the homeostasis of postsynaptic acetylcholine receptor packing at the neuromuscular junction.
- Densities of MuSK, activated Src kinase, phosphorylated ACh receptors and rapsyn were all reduced at motor endplates while β-dystroglycan was unaffected.
- Pulse-labelling showed that the slow decline in junctional ACh receptor density could be explained largely by diminished retention of ACh receptors within the postsynaptic membrane scaffold.
- The results suggest that anti-MuSK IgG reduces the density of MuSK, associated tyrosine phosphorylation and retention of junctional ACh receptors within the postsynaptic membrane.

Abstract Muscle-specific kinase (MuSK) autoantibodies from myasthenia gravis patients can block the activation of MuSK *in vitro* and/or reduce the postsynaptic localization of MuSK. Here we use a mouse model to examine the effects of MuSK autoantibodies upon some key components of the postsynaptic MuSK pathway and upon the regulation of junctional ACh receptor (AChR) numbers. Mice became weak after 14 daily injections of anti-MuSK-positive patient IgG. The intensity and area of AChR staining at the motor endplate was markedly reduced. Pulse-labelling of AChRs revealed an accelerated loss of pre-existing AChRs from postsynaptic AChR clusters without a compensatory increase in incorporation of (newly synthesized) replacement AChRs. Large, postsynaptic AChR clusters were replaced by a constellation of tiny AChR microaggregates. Puncta of AChR staining also appeared in the cytoplasm beneath the endplate. Endplate staining for MuSK, activated Src, rapsyn and AChR were all reduced in intensity. In the tibialis anterior muscle there was also evidence that phosphorylation of the AChR β-subunit-Y390 was reduced at endplates. In contrast, endplate staining for β-dystroglycan (through which rapsyn couples AChR to the synaptic basement membrane) remained intense. The results suggest that anti-MuSK IgG suppresses the endplate density of MuSK, thereby down-regulating MuSK signalling activity and the retention of junctional AChRs locally within the postsynaptic membrane scaffold.

(Received 19 December 2013; accepted after revision 11 May 2014; first published online 23 May 2014)
Corresponding author W. D. Phillips: School of Medical Sciences (Physiology) and Bosch Institute, Anderson Stuart Bldg (F13), University of Sydney, NSW 2006, Australia. Email: william.phillips@sydney.edu.au

Abbreviations AChR, acetylcholine receptor; AM, anti-MuSK patient IgG; α-BGT, α-bungarotoxin; β-DG, β-dystroglycan; LRP4, lipoprotein receptor-related protein 4; MG, myasthenia gravis; MuSK, muscle-specific kinase; NMJ, neuromuscular junction; TA, tibialis anterior (muscle).

DOI: 10.1113/jphysiol.2013.270207

Introduction

While most cases of myasthenia gravis (MG) are caused by autoantibodies that target the AChR, a subset of MG patients instead possess plasma antibodies against MuSK (Hoch 2001; McConville *et al.* 2004) or its partner protein, low density lipoprotein receptor related protein-4 (LRP4) (Higuchi *et al.* 2011; Pevzner *et al.* 2011; Shen *et al.* 2013). Rabbits, mice or rats developed myasthenic weakness after they were actively immunized with the extracellular domain of MuSK or were repeatedly injected with IgG from anti-MuSK-positive patients (Shigemoto *et al.* 2006; Cole *et al.* 2008; Richman *et al.* 2011; Klooster *et al.* 2012). In these experimental animals myasthenic weakness was associated with reduced postsynaptic AChR numbers at the neuromuscular junction (NMJ). Unlike classic anti-AChR MG, MuSK autoantibodies were predominantly of the IgG4 subtype and endplates did not reveal substantial T-lymphocyte- or complement-associated immunopathology (McConville *et al.* 2004; Shiraishi *et al.* 2005; Ohta *et al.* 2007; Klooster *et al.* 2012; Mori *et al.* 2012a). The easiest explanation of these findings is that MuSK autoantibodies impair the NMJ by interfering with the physiological role of MuSK in synapse maintenance.

MuSK is a receptor tyrosine kinase essential for the development of the mouse NMJ (Glass *et al.* 1996). During development, neural agrin, a proteoglycan released from the motor nerve terminal, binds to LRP4 on the muscle cell membrane. The LRP4–agrin complex assembles with MuSK, initiating signalling cascades that form and stabilize developing postsynaptic specializations (Kim *et al.* 2008; Zhang *et al.* 2008). The cytoplasmic scaffolding protein Dok7 assembles to help stabilize the catalytically active MuSK dimer (Bergamin *et al.* 2010). MuSK also has some intrinsic kinase activity (in the absence of agrin) and the level of MuSK gene expression was a critical determinant of the number and location of AChR clusters and NMJs on developing muscle fibres, independent of the nerve (Kim & Burden, 2008).

Perhaps the best understood signalling pathway downstream of MuSK involves non-receptor tyrosine kinases Abl and Src. Activation of MuSK by neural agrin causes phosphorylation of Abl and Src kinase and the AChR β-subunit (βY390) (Finn *et al.* 2003; Mittaud *et al.* 2004). Abl activation provides positive feedback by prolonging and enhancing the phosphorylation of MuSK itself (Finn *et al.* 2003). Src is known to bind the large intracellular loop of the AChR β-subunit (Fuhrer & Hall, 1996). Abl and Src both help drive phosphorylation of AChR-βY390. The Src-family kinases (Src, Fyn and Yes) are not essential for AChR clustering in cultured muscle cells but Src does help to immobilize AChRs in the membrane (Mittaud *et al.* 2001; Mohamed *et al.* 2001; Sadasivam *et al.* 2005).

Rapsyn, a cytoplasmic scaffolding protein, is essential for AChR clustering (Gautam *et al.* 1995). High-resolution (4 Å) electron microscopic imaging of postsynaptic membranes from the *Torpedo* electric organ showed that the cytoplasmic face of each AChR pentamer was decorated by a variable number (up to 3) of radially protruding lobes/struts (Zubera & Unwin, 2013). Each strut was thought to be a single rapsyn molecule. In portions of the membrane where AChRs were tightly packed (10^4 AChR μm^{-2}) adjacent AChRs were held together by interactions between their protruding rapsyn struts. Studies with recombinant rapsyn are consistent with this cross-linking function. Rapsyn can form a coiled-coil interaction with the AChR and can self-associate via its tetratricopeptide repeats (Ramarao & Cohen, 1998; Bartoli *et al.* 2001; Ramarao *et al.* 2001; Huebsch & Maimone, 2003; Lee *et al.* 2009). Phosphorylation of AChR-βY390 is known to recruit an additional rapsyn molecule to bind each AChR pentamer (Borges & Ferns, 2001; Moransard *et al.* 2003; Borges *et al.* 2008). Thus, reversible phosphorylation of AChR-βY390 might regulate the number of rapsyn struts per AChR, and consequently AChR aggregation. Dystroglycan also helps to stabilize postsynaptic AChR clusters (Cote *et al.* 1999; Jacobson *et al.* 2001; Kahl & Campanelli, 2003; Lefebvre *et al.* 2007). The carboxyl-terminal RING-H2 domain of rapsyn binds to β-dystroglycan (β-DG; Cartaud *et al.* 1998; Fuhrer *et al.* 1999; Bartoli *et al.* 2001). Thus rapsyn may link AChR microaggregates, via β-DG, into large postsynaptic membrane scaffolds that are organized by the overlying synaptic basement membrane (McMahan & Slater, 1984). Overexpression of rapsyn in adult muscle, which forced an increase in the endplate rapsyn/AChR ratio, had the effect of stabilizing postsynaptic AChRs, presumably by favouring increased rapsyn interactions (Gervásio & Phillips, 2005; Losen *et al.* 2005).

Recent *in vitro* studies have identified several ways in which anti-MuSK IgG can interfere with MuSK. Firstly, some sources of bivalent anti-MuSK IgG were found to chronically activate MuSK (Hopf & Hoch, 1998; Shigemoto *et al.* 2006; Cole *et al.* 2010; Mori *et al.* 2012b). Secondly, anti-MuSK patient IgG was reported to disrupt the interaction between MuSK and collagen Q, and this was associated with reduced endplate staining for both proteins (Kawakami *et al.* 2011; Ohno *et al.* 2013). Thirdly, anti-MuSK IgG4 inhibited the interaction between LRP4 and MuSK (Klooster *et al.* 2012; Huijbers *et al.* 2013; Koneczny *et al.* 2013). These findings suggest that MuSK autoantibodies acutely interfere with the postsynaptic localization of MuSK, or its physiological activation, or both. AChR clusters formed in cell culture were rapidly disrupted by anti-MuSK IgG. In contrast, mice injected daily with anti-MuSK patient IgG displayed a gradual, steady decline in endplate AChR density over 2 weeks

(Morsch *et al.* 2012). Here we report that repeated injections of anti-MuSK patient IgG suppressed endplate levels of MuSK, activated Src, phosphorylated AChRs and rapsyn. The steady decline in endplate AChR density could be largely explained by accelerated detachment of pre-existing AChRs from the postsynaptic membrane scaffold.

Methods

Ethical approval

The article by G. B. Drummond (Drummond, 2009) was read carefully to be sure that our experiments complied with the policies and regulations regarding animal experimentation and other ethical matters. A total of 24 mice were killed specifically for use in this study. We also used muscles of 33 mice from previously reported studies. All mouse experiments described in this paper were conducted with the approval of the University of Sydney Animal Ethics Committee in compliance with the NSW Animal Research Act 1985 and the *Australian Code of Practice for the Care and Use of Animals for Scientific Purposes* (7th Edition, NHMRC 2004). Patient consent was obtained in accordance with the *Declaration of Helsinki*. The project was approved by the Human Research Ethics Committee of the Sydney South West Area Health Service.

Injection of anti-MuSK-positive patient IgG

The mouse model was described previously (Cole *et al.* 2008, 2010; Morsch *et al.* 2012). Six-week-old female C57BL/6J mice (Animal Resources Centre, Western Australia) were group housed in filter-top cages with wire-grid lids (17 cm × 34 cm × 13 cm; W × L × H). Mice had free access to water and Glen Forrest Rat and mouse cubes (Glen Forrest, Western Australia). They received a series of daily I.P. injections of total IgG from anti-MuSK-positive MG patients dissolved in sterile PBS. A single injection of cyclophosphamide monohydrate (300 mg kg^{-1} I.P.; Sigma, St Louis, MO, USA) was also given 24 h after the first IgG injection to suppress any active immune response to the human proteins (Toyka *et al.* 1977). Batches of anti-MuSK-positive patient IgG (AM) were numbered as previously described (Cole *et al.* 2010; Morsch *et al.* 2013). Table 1 details the batches injected and the weakness grades produced in mice. The mice injected with AM4.4, AM4.5 and AM5 were vehicle-control mice from another study (Morsch *et al.* 2013). On day 8 of the IgG injection series a subcutaneous osmotic minipump was implanted that delivered systemically 11.8 μl h^{-1} of mestinon buffer solution (in mM: citric acid monohydrate 1.3, sodium citrate dehydrate 4.1, methyl paraben 0.5, propyl paraben 0.05 and NaCl 7.4). Mice injected with AM2, AM5 and AM4.5 were compared to control mice that received daily injections of control human IgG that was negative for both MuSK and AChR autoantibodies. Mice injected with AM4.4 IgG were compared to naive (control) mice of the same age. Mice were killed with pentobarbitone (30 mg I.P.; CenVet Australia).

Immunostaining and confocal imaging

To measure the size of AChR clusters, 20 μm longitudinal sections were labelled with Alexa555-α-bungarotoxin. *En face* confocal *Z*-projection images of endplates were obtained and analysed as previously described (Cheng *et al.* 2013). Briefly, NIH ImageJ was used to apply a threshold so as to isolate discrete areas of bright staining and measure their area. Depending upon the size, these areas were described as either AChR clusters or AChR microaggregates. For immunostaining, transverse cryosections (12 μm) of the tibialis anterior (TA) and diaphragm muscles were fixed on slides with 2% paraformaldehyde in PBS for 15 min then washed three times with PBS over 30 min. Immunofluorescent staining for MuSK was conducted as described previously (Cole *et al.* 2010). When staining with anti-phospho-peptide antibodies, phosphatase inhibitor cocktail no. 2 (1:100, Sigma) was included in the 2% paraformaldehyde solution. Sections were pre-blocked in 2% bovine serum albumin (BSA), 0.1% Triton X-100 in PBS for 1 h at room temperature. All antibodies were diluted in 2% BSA in PBS. Total Src was detected with monoclonal rabbit anti-Src monoclonal antibody that is likely to cross-react with several other members of the extended Src family (1:200 EG107, Abcam). Activated Src was detected with affinity-purified rabbit antibody against the tyrosine-phosphorylated form of the conserved activation loop (1:200 anti-phospho-Src-Y418; Sigma) hereafter referred to as activated Src (Boggon & Eck, 2004). Polyclonal rabbit anti-phospho-AChR-βY390 was diluted 1:250 (Santa Cruz Biotechnology, Santa Cruz CA, USA), affinity-purified sheep anti-MuSK extracellular domain antibody was diluted 1:100 (Cole *et al.* 2010). Affinity-purified tetramethylrhodamine isothiocyanate-conjugated donkey anti-sheep IgG was diluted 1:250 (H+L; Jackson Labs, Baltimore, PA, USA). AChRs were labelled by adding 1:200 Alexa488-α-bungarotoxin (Alexa488-α-BGT; Molecular Probes, Eugene OR, USA).

For triple-labelling, sections were incubated overnight at 4°C with a mixture of 1:1000 affinity-purified rabbit anti-β-DG (a kind gift from Dr Vann Bennett, Ayalon *et al.* 2008) and 1:100 fluorescein isothiocyanate-conjugated monoclonal mouse anti-rapsyn (mab1234 Peng & Froehner, 1985; Millipore, Billerica MA, USA). Sections were then washed three times with PBS over

30 min and incubated with a mixture of 1:250 Cy3-conjugated, affinity-purified donkey anti-rabbit IgG (Jackson ImmunoResearch, Baltimore MD, USA) and 1:200 Alexa647-α-bungarotoxin (Alexa647-α-BGT; Molecular Probes) for 1 h at room temperature. Coverslips were mounted with polyvinyl alcohol mounting medium containing 1,4-diazabicyclo[2.2.2]octane to prevent fading (Sigma-Aldrich). All sections were imaged on a Zeiss LSM 510 Meta confocal microscope using a $\times$40 1.2 NA air objective. ImageJ software was used to measure the area and relative intensity of endplate immunofluorescence as described previously (Cole *et al.* 2008, 2010).

To facilitate the reproduction of immunostaining figures, the brightness and/or contrast was increased as specified in the figure legend. Where this was done, the same percentage adjustment was applied to both control and experimental images.

Pulse-labelling and turnover of endplate AChRs

Mice were anaesthetized with 2% isoflurane/oxygen and the lateral surface of the TA muscle was surgically exposed and incubated with Alexa555-α-BGT (10 μg ml^{-1}, Molecular Probes) for 1 h. Unbound Alexa555-α-BGT was removed by washing 3 times with PBS. This exposure was sufficient to completely block subsequent binding of Alexa647-α-BGT to the Alexa555-α-BGT-labelled endplate (N. Ghazanfari, unpublished observations). The skin was then closed and sutured. The mice received a single subcutaneous injection of buprenorphine for analgesia (0.03 mg kg^{-1}; Reckitt Benckiser, Australia) immediately, and again the following day. After recovery from anaesthesia mice received six daily I.P. injections of control human IgG or AM4.5 (45 mg day^{-1}). On day 6 the mice were again anaesthetized and the muscle was again exposed. Newly synthesized AChRs, inserted on the fibre surface between days 0 and 6, were labelled with Alexa647-α-BGT (10 μg ml^{-1}, Molecular Probes), as above. After washing the muscle surface 3 times with PBS, the mouse was killed with pentobarbitone (30 mg I.P.; CenVet Australia). The muscle was then dissected and fixed with 4% paraformaldehyde in PBS for 30 min. Fascicles of muscle fibres teased from the surface of the muscle were transferred to slides. Additional naive mice were labelled as above with either Alexa555-α-BGT or Alexa647-α-BGT for 1 h and were killed immediately to permit normalization of endplate fluorescence intensities (pre-existing AChRs = 100%). *En face* images of endplates were collected as confocal *Z*-projections. Experimental and control images were all collected in the same imaging session, using fixed gain and black-level settings (Zeiss LSM510 Meta confocal microscope). Metamorph software (Molecular Devices, Inc., CA, USA) was used to split the colour channels and an intensity threshold was set to isolate the region of interest from background. Metamorph's integrated morphometry analysis tool was used to measure the area and intensity of the postsynaptic AChR clusters. The integrated pixel intensity was then calculated as the sum of pixel intensities for all suprathreshold pixels within a boundary line drawn to delimit the endplate in question. Previous work indicates that the intensity of α-bungarotoxin fluorescence in these *Z*-projection images provides a reliable measure of differences in the local density of AChRs among endplates. In mice receiving a series of 14 daily injections of anti-MuSK-positive IgG the autoantibody caused a steady 3% per day decline in α-bungarotoxin fluorescence. This was matched by a 3% per day decline in miniature endplate potential amplitude, an independent measure of relative AChR density (Morsch *et al.* 2012).

Statistical analysis

GraphPad Prism (GraphPad Software, CA, USA) was used for statistics. Data in the text is presented as mean $\pm$ SEM. Unless otherwise indicated, comparisons of two groups were by unpaired, two-tailed Student's *t* test (anti-MuSK-injected *versus* control mice), where *n* was the number of mice per treatment group. Significance is indicated throughout as follows: $^{*}P < 0.05$, $^{**}P < 0.01$, $^{***}P < 0.001$.

Results

Table 1 describes the batches of anti-MuSK-positive patient IgG (AM2, AM4.4, AM4.5 and AM5) and their functional impact upon the mice. The mice that received 14 daily injections of AM4.4 or AM4.5 were from previous electrophysiological studies that demonstrated reductions in the amplitudes of the endplate potential and spontaneous miniature endplate potential in the diaphragm muscle (Morsch *et al.* 2012, 2013). The mice injected with AM2, AM4.4 or AM5 all displayed whole-body weakness and weight loss (Cole *et al.* 2008; Morsch *et al.* 2012, 2013).

Anti-MuSK antibodies cause remodelling of endplate AChR clusters

When viewed *en face*, motor endplates of healthy control mice typically consisted of one or two contiguous AChR-rich areas (AChR clusters) often with pretzel-like boundaries (Fig. 1*A*). In mice that had become weak after 14–15 daily injections of anti-MuSK-positive patient IgG, the endplate instead often consisted of a constellation of AChR microaggregates (Fig. 1*B*). Since large AChR clusters grow by the reversible coalescence of AChR microaggregates (Pumplin & Bloch, 1987;

Table 1. Batches of human IgG injected and resultant mouse weakness

Patient number	IgG batch number	Dose injected (mg day^{-1})	MGFA grade[a]	Weakness grade of mice[b]
2	AM2	45	4B (severe)	2.0
5	AM5	20	4B (severe)	2.0
4	AM4.4	45	4B (severe)	1.6[e]
4	AM4.5	25[d]	3B (moderate)	0[e]
Control[c]	pooled	45	N/A	0

[a]MGFA, Myasthenia Gravis Foundation of America score of patient at time of plasma collection. [b]Average weakness grade produced in mice at the end of the IgG injection series (14–15 days) according to the grading scheme of Stacy *et al.* (2002). The mice injected with AM4.4, AM4.5 and AM5 were vehicle-control mice from another study (Morsch *et al.* 2013). See Methods for details. [c]Control IgG was from pooled plasma from therapeutic venesection of haemochromatosis patients screened negative for both anti-AChR and anti-MuSK. [d]For the AChR pulse-labelling experiments 45 mg day^{-1} of AM4.5 IgG was injected. [e]For these particular mice we previous recorded endplate potentials in the diaphragm muscle. The amplitudes of endplate potentials and miniature endplate potentials were significantly reduced, compared to healthy control mice (Morsch *et al.* 2012, 2013).

Weston *et al.* 2003; Ngo *et al.* 2012) we measured the size of the individual AChR clusters/aggregates. Figure 1*C* shows the distribution of AChR cluster sizes pooled from endplates of healthy control diaphragm muscles. Healthy endplates displayed both large AChR clusters (>4 μm) and tiny AChR microaggregates (<2 μm). In the diaphragm muscle, endplates contained an average of one large AChR cluster (Fig. 1*D*, open bars) plus 1-2 AChR microaggregates (Fig. 1*E*, open bars). Endplates in the healthy TA muscle typically contained more AChR clusters/aggregates than those in the healthy diaphragm (Fig. 1*D* and *E*, compare open bars). Following the series of injections of anti-MuSK-positive patient IgG, the number of large AChR clusters was significantly reduced in both muscles (Fig. 1*D*, black bars). This was reflected in similar reductions in the total AChR-rich area per endplate (Fig. 1*F*). AChR microaggregates survived. In the diaphragm muscle AChR microaggregates became significantly more numerous after the anti-MuSK IgG injections (Fig. 1*E*). In the healthy diaphragm muscle the tiny AChR microaggregates amounted to just 1.5% of the total AChR area of the endplate. In mice injected with AM4.4 IgG, AChR microaggregates came to represent 37% of the (much diminished) total AChR area (24% for mice injected with AM5). Thus anti-MuSK IgG selectively hindered the maintenance of large AChR clusters.

Anti-MuSK antibodies modified turnover of AChRs at endplate clusters

The effect of anti-MuSK patient IgG upon the metabolic turnover of endplate AChRs was studied in the TA muscle of 8-week-old living mice (Fig. 2*A*). Endplate AChRs that were present on day 0 were pulse-labelled with Alexa555-α-BGT (Fig. 2*B*; pre-existing AChRs). Residual Alexa555-α-BGT fluorescence was also imaged at endplates from mice that received six daily injections of control IgG (Fig. 2*D*) or AM4.5 IgG (Fig. 2*G*). Integrated pixel intensity measurements (fluorescence intensity × area) showed that in mice injected with AM4.5, endplate AChR clusters lost 75 ± 5% ($n = 4$ mice) of their pre-existing AChRs over the 6 days, compared to just 34 ± 14% ($n = 4$ mice) loss in control mice (Fig. 2*J*; $P = 0.03$, unpaired Student's *t* test). Newly incorporated, replacement AChRs were detected at the same endplates with Alexa647-α-BGT (Fig. 2*E* and *H*). After 6 days of AM4.5 IgG injections, newly inserted AChRs amounted to 35 ± 10% ($n = 4$ mice) of the original endplate complement. This was not significantly less than the 52 ± 8% value ($n = 4$ mice) for newly incorporated AChRs received at endplates in control mice (Fig. 2*K*; $P = 0.22$). By subtracting the loss of pre-existing AChRs from the gain of replacement AChRs we made an estimate that endplates of the mice injected with AM4.5 IgG would have suffered a net 40% reduction in their AChR complement over 6 days (6.6% per day), due to the changes in turnover (Fig. 2*J* and *K*). This estimate, though very approximate, is consistent with the measured rate of decline of total AChR per endplate (intensity × area) for the gastrocnemius and diaphragm muscles of mice injected with IgG from the same patient (Fig. 2*L*; Morsch *et al.* 2012). Thus, the progressive anti-MuSK-induced decline in endplate AChR number could be explained by impaired retention of AChRs within AChR clusters, without a compensatory increase in replacement AChRs.

Optical sections transverse to the muscle fibres provided a closer view of the subcellular distribution of AChRs. Healthy endplates appeared as a discrete crescent of AChR staining (Fig. 3*A*). In mice injected with anti-MuSK IgG, crescents of endplate AChR staining were still present, but were dimmer and tiny puncta of AChR staining often appeared in the cytoplasm beneath the endplate (arrow in Fig. 3*B* and *G*). Subsynaptic puncta of AChRs were not found beneath healthy control endplates (Fig. 3*A*, *C*, *E* and *G*). The fraction of endplates with subsynaptic puncta of AChR staining increased during the anti-MuSK IgG injection series in the omohyoid, masseter, TA and sternomastoid muscles (Fig. 3*H*). In the mice injected with AM4.5 IgG, puncta of internalized AChRs could be detected beneath some endplates (Fig. 3*F*). It is not clear whether internalized AChRs account for all of the AChR puncta observed

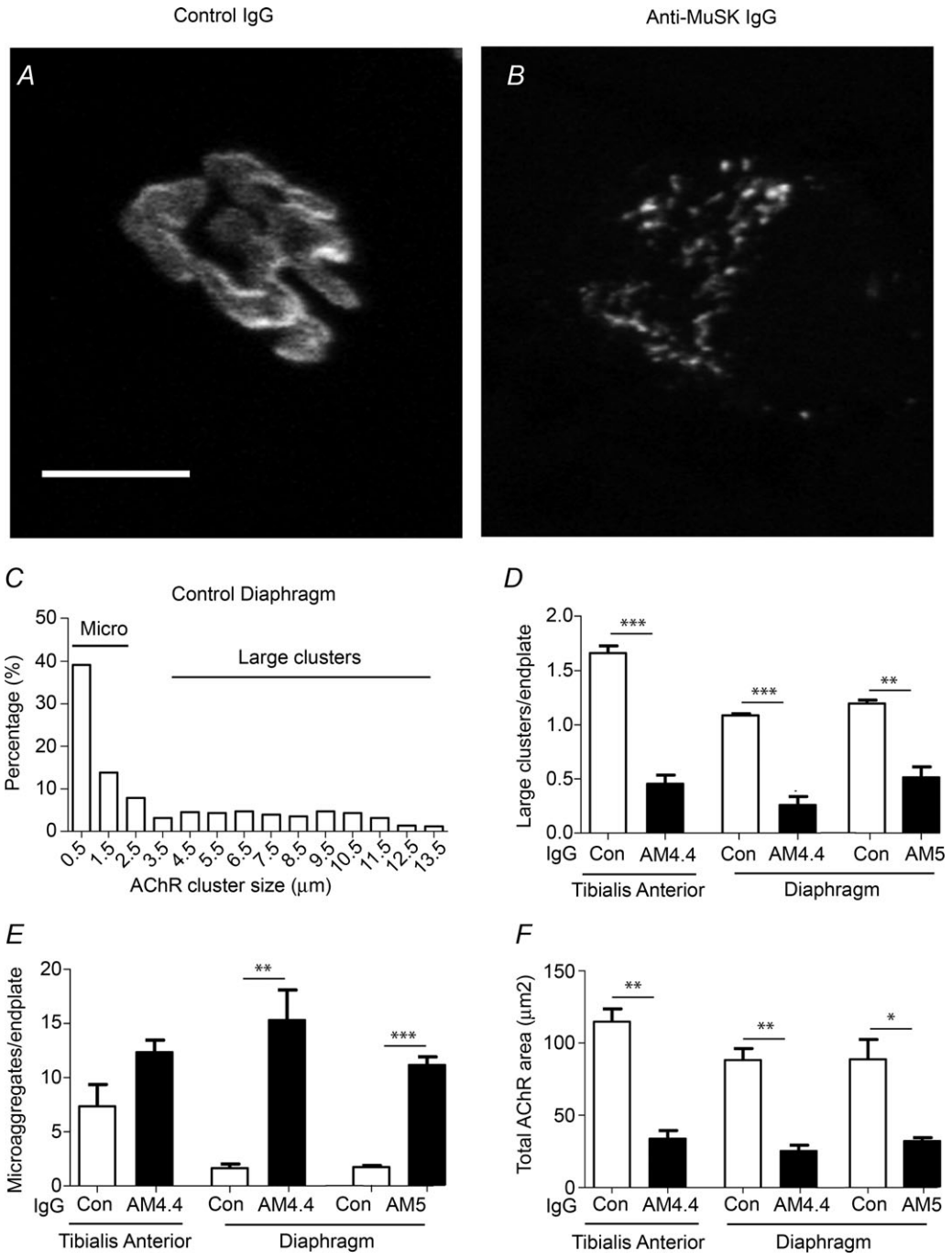

Figure 1. Anti-MuSK antibodies remodel endplate AChR clusters
A, *en face* confocal *Z*-projection image showing a large, pretzel-shaped AChR cluster at an endplate in the healthy diaphragm muscle. The mouse had received 15 daily injections of control IgG. AChRs were labelled with Alexa555-α-BGT. Scale bar, 10 μm. *B*, myasthenic endplate from the diaphragm muscle of a mouse that received 15 daily injections of AM5 IgG. The endplate consists mostly of tiny AChR microaggregates. *C*, frequency histogram showing the sizes of discrete AChR clusters pooled from endplates in diaphragm muscles of healthy control mice. Size is expressed as the square root of the measured AChR cluster area. Numbers on the abscissa indicate the centre of each bin. Large AChR clusters were arbitrarily defined as those $\geq$4 μm (area $\geq$16 μm^2) while those $\leq$2 μm (area $\leq$4 μm^2) were defined as AChR microaggregates (Micro). *D*, number of large AChR clusters per endplate in the TA and diaphragm muscles after 15 daily injections of control human IgG (Con), AM4.4 IgG or AM5 IgG. *E*, number of AChR microaggregates per endplate. *F*, total area of clustered AChRs per endplate. Open bars represent control mice while filled bars represent mice injected with AM4.4 IgG or AM5 IgG. Bars in panels *D*–*F* represent the mean + SEM for $n = 3$ mice ($^*P < 0.05$, $^{**}P < 0.01$, $^{***}P < 0.001$, unpaired Student's *t* test).

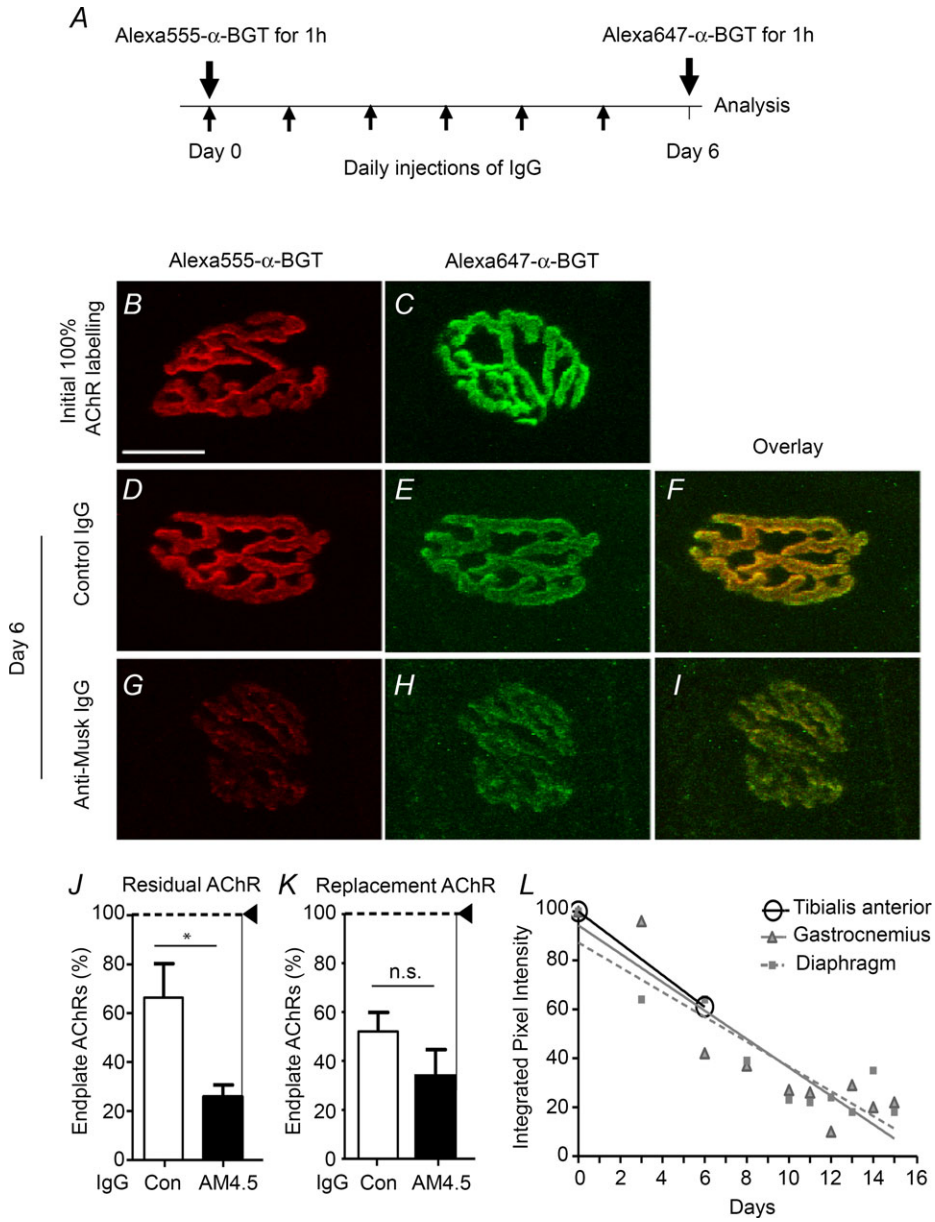

Figure 2. Anti-MuSK IgG modifies the turnover of endplate AChRs
A, AChRs on the surface of the TA muscle were pulse-labelled with Alexa555-α-BGT on day 0. After 6 daily injections of control IgG or AM4.5 IgG, newly inserted replacement AChRs were labelled with Alexa647-α-BGT. *B*, saturation labelling of endplate AChRs on day 0 with Alexa555-α-BGT (initial 100% AChR labelling). Scale bar, 20 μm. *C*, saturation endplate labelling with Alexa647-α-BGT viewed on day 0 (100% of AChRs). *D–F*, an endplate imaged after 6 daily injections of control IgG showing: residual Alexa555-α-BGT fluorescence (*D*), newly inserted AChRs labelled on day 6 with Alexa647-α-BGT (*E*), overlay of the two fluorescence channels (*F*). *G–I*, an endplate imaged after 6 daily injections of AM4.5 IgG showing: residual Alexa555-α-BGT fluorescence (*G*), newly inserted AChRs labelled on day 6 with Alexa647-α-BGT (*H*), overlay (*I*). The brightness and contrast was increased in equal proportion for control and experimental panels to facilitate reproduction. *J*, percentage loss of Alexa555-α-BGT-labelled endplate AChRs between days 0 and 6 (fluorescence intensity × area). The open bar shows results for control IgG (Con) while the black bar represents mice injected with AM4.5 IgG. *K*, newly synthesized AChRs added to endplate AChR clusters between days 0 and 6, as a percentage of the original complement of endplate AChRs. Bars represent the mean + SEM for $n = 4$ mice (*$P < 0.05$; unpaired Student's *t* test). *L*, measured declines in the net amount of AChRs at endplates in the gastrocnemius (triangles) and diaphragm (squares) muscles of mice receiving daily injections of IgG from the same patient (Morsch *et al.* 2012). Endplate AChR complement is expressed in terms of integrated pixel intensities, normalized to the day 0 (100%) value. Open circles show our estimated drop in endplate AChR complement for mice injected with AM4.5 IgG, calculated by subtracting the percentage loss of original AChRs (*J*) from the percentage gain of replacement AChRs (*K*).

beneath endplates in the anti-MuSK-injected mice. In the diaphragm muscle the effects of the anti-MuSK IgG injections were subtly different. AChRs were no longer confined within discrete endplate AChR crescents. Instead puncta of AChR staining spread around the muscle fibre circumference (Fig. 3*D*, arrow indicates a fragmented AChR cluster). This dispersed pattern of AChR puncta was a common phenomenon in the diaphragm muscle, but was relatively uncommon in the other muscles examined (Fig. 3*I* and *J*).

Rapsyn and AChR are displaced from the dystroglycan-rich endplate

In triple-labelled sections of muscles from control mice, AChRs and rapsyn were strongly concentrated together at the endplate (Fig. 4*A* and *B*). As expected, β-DG immunostaining was present throughout the sarcolemma but was concentrated at the endplate (Fig. 4*C*). In mice that became weak after injections of either AM2 IgG or AM5 IgG, endplate staining for AChR and rapsyn were both markedly dimmer compared to control mice (Fig. 4*D* and *E*). In contrast β-DG staining of endplate crescents remained bright (Fig. 4*F*). This selective reduction in endplate staining for AChRs and rapsyn (but not β-DG) was confirmed by quantification of endplate staining intensities in both the TA and diaphragm muscles (Fig. 4*G* and *H*, horizontal dashed line represents staining intensities for control mice). The reduction in AChR staining intensity appeared to be slightly greater than for rapsyn staining, consistent with previous findings (Cole *et al.* 2010). In summary, injections of anti-MuSK IgG selectively displaced AChR and rapsyn (but not β-DG) from the endplate.

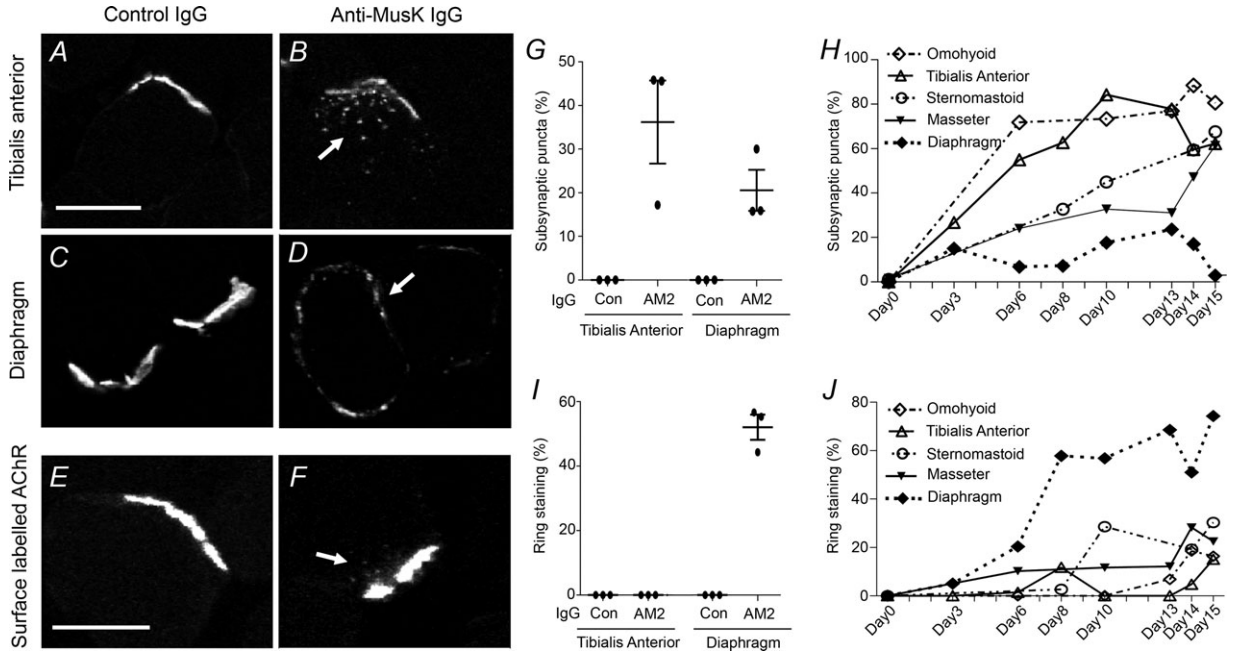

Figure 3. Subcellular redistribution of AChRs at endplates after injections of anti-MuSK IgG
A, an endplate from the TA muscle of a control mouse stained for AChRs and viewed in transverse section appears as a crescent. *B*, an endplate stained for AChRs after 14 daily injections of AM2 IgG. Puncta of AChR staining appear in the cytoplasm beneath the endplate AChR crescent (arrow). *C*, two crescent-shaped endplates from the diaphragm muscle of a control mouse. *D*, remnants of an endplate in the diaphragm muscle after 14 daily injections of AM2 IgG. A ring of AChR staining is spread around the muscle fibre circumference. The fragmented endplate AChR crescent is marked by an arrow. *E*, a healthy endplate from the TA muscle after pulse-labelling of cell surface AChRs and 6 daily injections of control IgG (as per Fig. 2). Surface AChRs remain concentrated at the crescent-shaped endplate. *F*, an endplate from the TA muscle after pulse-labelling of cell surface AChRs and 6 daily injections of AM4.5 IgG. Puncta of internalized AChR staining are indicated by the arrow. Scale bars for panels *A–D* and *E* and *F* are 20 μm. The brightness and contrast were increased in equal proportion for control and experimental panels to facilitate reproduction. *G*, percentage of endplates displaying subsynaptic AChR puncta after 14 daily injections of AM2 IgG. Symbols show results for individual mice while bars represent the mean $\pm$ SEM. *H*, time-course for the appearance of subsynaptic puncta in the indicated muscles during a series of daily injections of AM4.4 IgG. One mouse was analysed at each indicated time-point. *I*, percentage of endplates displaying a ring of sarcolemmal staining after 14 daily injections of AM2 IgG or control IgG. *J*, time-course for the appearance of a ring of sarcolemmal staining in the indicated muscles during a series of daily injections of AM4.4 IgG.

Anti-MuSK antibodies depress MuSK pathway markers at the endplate

In control muscles MuSK was concentrated with AChRs at the endplate (Fig. 5*A* and *B*). After 15 daily injections of anti-MuSK-positive IgG, endplate staining for both MuSK and AChR were significantly dimmer than for control mice (Fig. 5*C*–*E*). Within the boundaries of the residual MuSK-stained endplate crescents (Fig. 5*D*, arrows) AChR staining was often patchy, reflecting the break-up into AChR microaggregates (arrows in Fig. 5*C*).

We next examined the distribution of Src. In control mice, staining for total Src (monoclonal EG107) showed partial co-localization with AChRs but was also present

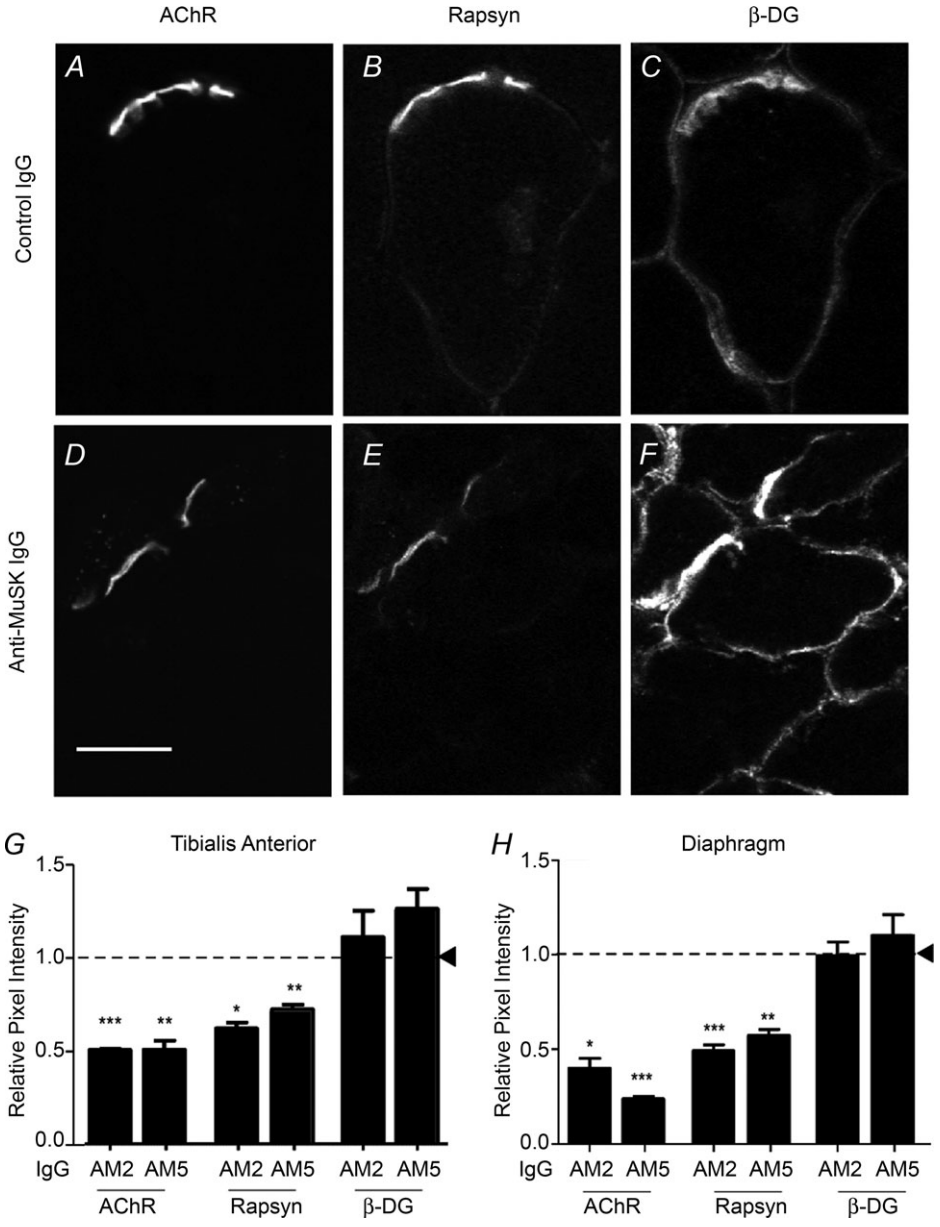

Figure 4. MuSK autoantibodies displace AChRs and rapsyn from the β-DG-rich endplate
A–*C*, an endplate from the TA muscle of a control mouse triple-labelled for AChRs (*A*), rapsyn (*B*) and β-DG (*C*). All three proteins are concentrated within the crescent-shaped endplate. *D*–*F*, two endplates from the TA muscle after 14 daily injections of AM2 IgG. Staining for AChRs and rapsyn were dimmer and incomplete, but β-DG staining of the endplate crescents remained strong. Scale bar in panel *D* is 20 μm. *G*, intensity of endplate staining for AChRs, rapsyn and β-DG in the TA muscle in mice after 14 daily injections of AM2 IgG or AM5 IgG. Intensity is expressed relative to mice injected with control human IgG (horizontal dashed line and arrowhead). *H*, comparable results for endplates from the diaphragm muscle. Data represent the mean + SEM for $n = 3$ mice ($^{*}P < 0.05$, $^{**}P < 0.01$, $^{***}P < 0.001$ compared to control mice; unpaired Student's *t* test).

in non-synaptic parts of the muscle fibre (Fig. 6*A*–*C*). By comparison, antibodies specific for the activated state of Src kinase (phospho-Src-Y418) showed a consistent co-distribution with AChRs at endplates (Fig. 6*D*–*F*). We therefore focused our quantitative analysis on staining for activated Src. In mice that became weak after injections of either AM2 IgG or AM5 IgG, endplate staining for activated Src was significantly dimmer, compared to control mice (Fig. 6*H* and *J*). These results suggest that the injections of anti-MuSK IgG caused a reduction in the density of activated Src at the endplate.

At healthy endplates immunostaining for phosphorylated AChR-βY390 was closely co-localized with total AChR (Alexa488-α-BGT staining) as would be expected (Fig. 7*A*–*C*). In the TA muscle of mice injected with anti-MuSK IgG, endplate staining for phospho-AChR-βY390 was less intense than in control mice (Fig. 7*D*–*G*). Indeed the phospho-AChR-βY390/total-AChR fluorescence intensity ratio was significantly reduced at endplates in the TA muscle of mice injected with anti-MuSK IgG (Fig. 7*I*). In contrast, endplates in the diaphragm muscle of the same mice revealed no significant change in the phospho-AChR-βY390/total-AChR fluorescence intensity ratio (Fig. 7*I*). These results suggest that anti-MuSK-positive patient IgG reduced the phosphorylated fraction of AChRs at endplates in the TA muscle.

In cultured myotubes Abl kinase is a necessary component of the MuSK pathway of AChR clustering (Finn *et al.* 2003; Mittaud *et al.* 2004), yet the anti-cancer drug imatinib (Gleevec) is an Abl kinase inhibitor. We therefore tested whether Gleevec might show myasthenic side effects at clinically relevant doses. Three times daily injections of 50 mg kg^{-1} Gleevec were reported to halve the levels of activated Abl kinase and inhibit tumour growth in mice (le Coutre *et al.* 1999). After 14 days of the same (therapeutically relevant) Gleevec dosage we found no significant change in the intensity of endplate staining for activated Src, total AChR or phospho-AChR-βY390 staining (N. Ghazanfari, unpublished observations).

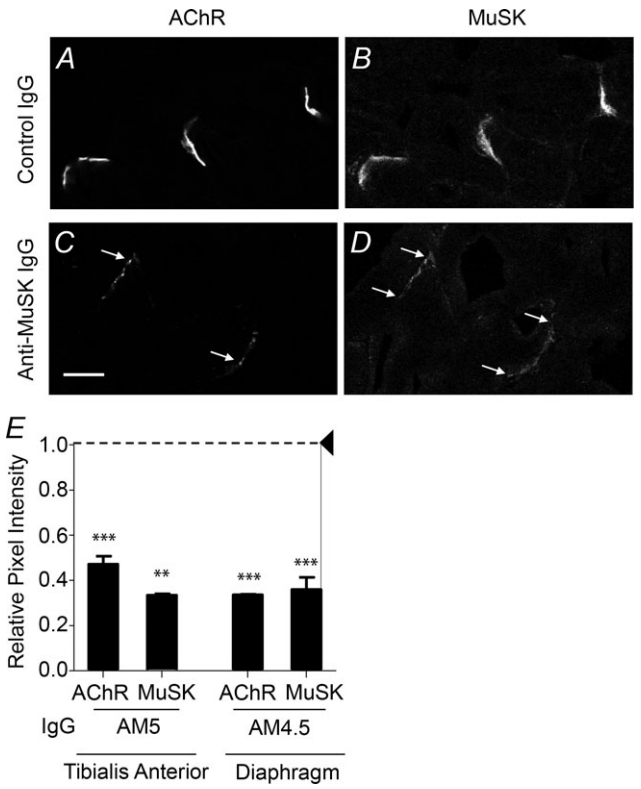

Figure 5. Anti-MuSK antibodies reduced endplate staining for MuSK
A and *B*, three healthy endplates from the TA muscle of a control mouse double-labelled for AChR (*A*) and MuSK (*B*). *C* and *D*, two endplates from the TA muscle of a mouse after 15 daily injections of AM5 IgG showing dim staining for both AChR (*C*) and MuSK (*D*). Scale bar in panel *C* is 20 μm. The brightness and contrast were increased in equal proportion for control and experimental panels for reproduction. *E*, intensity of endplate staining for AChR and MuSK after 15 daily injections of either AM5 or AM4.5 IgG. Endplate fluorescence intensities are expressed relative to those from control mice (horizontal dashed line and arrowhead). Bars represent the mean + SEM for $n = 3$ mice injected with AM5 IgG, and $n = 4$ mice injected with AM4.5 IgG (**$P < 0.01$, ***$P < 0.001$ compared to control mice; unpaired Student's *t* test).

Discussion

At present there is insufficient evidence from human biopsy studies to identify the molecular changes responsible for neuromuscular transmission failure in anti-MuSK-positive MG patients (Selcen *et al.* 2004; Niks *et al.* 2010), forcing us to rely tentatively upon findings in animal and cell culture models. Recent *in vitro* experiments revealed three immediate impacts of MuSK autoantibody binding upon MuSK itself: (1) some bivalent anti-MuSK IgG preparations cross-linked MuSK dimers causing non-physiological activation of MuSK (Hopf & Hoch, 1998; Shigemoto *et al.* 2006; Cole *et al.* 2010); (2) anti-MuSK patient IgG preparations disrupted the binding of MuSK to collagen Q, which might impair the synaptic localization of both MuSK and collagen Q (Kawakami *et al.* 2011; Ohno *et al.* 2013); (3) anti-MuSK IgG4 patient antibodies prevented the binding of LRP4 to MuSK, thereby blocking MuSK activation (Huijbers *et al.* 2013; Koneczny *et al.* 2013). Each of these actions of the autoantibodies might be expected to impair physiological MuSK signalling at the endplate. The present work addresses the longer-term effects of anti-MuSK patient IgG *in vivo*. We show that ongoing exposure of endplates to anti-MuSK patient IgG reduced staining levels for MuSK and its downstream effectors. The most pronounced effect was an accelerated loss of pre-existing AChRs from

postsynaptic AChR clusters. This loss was not balanced by any compensatory increase of newly synthesized, replacement AChRs.

The steady-state number of junctional AChRs depends upon the rate at which newly synthesized AChRs are incorporated into endplate AChR clusters minus the rate at which older AChRs are removed and degraded (Akaaboune *et al.* 1999, 2002). Our pulse-labelling experiments in control mice showed that the pre-existing AChRs lost from the endplate over 6 days were completely replaced by newly synthesized AChRs. However, endplates of mice injected with AM4.5 IgG lost significantly more

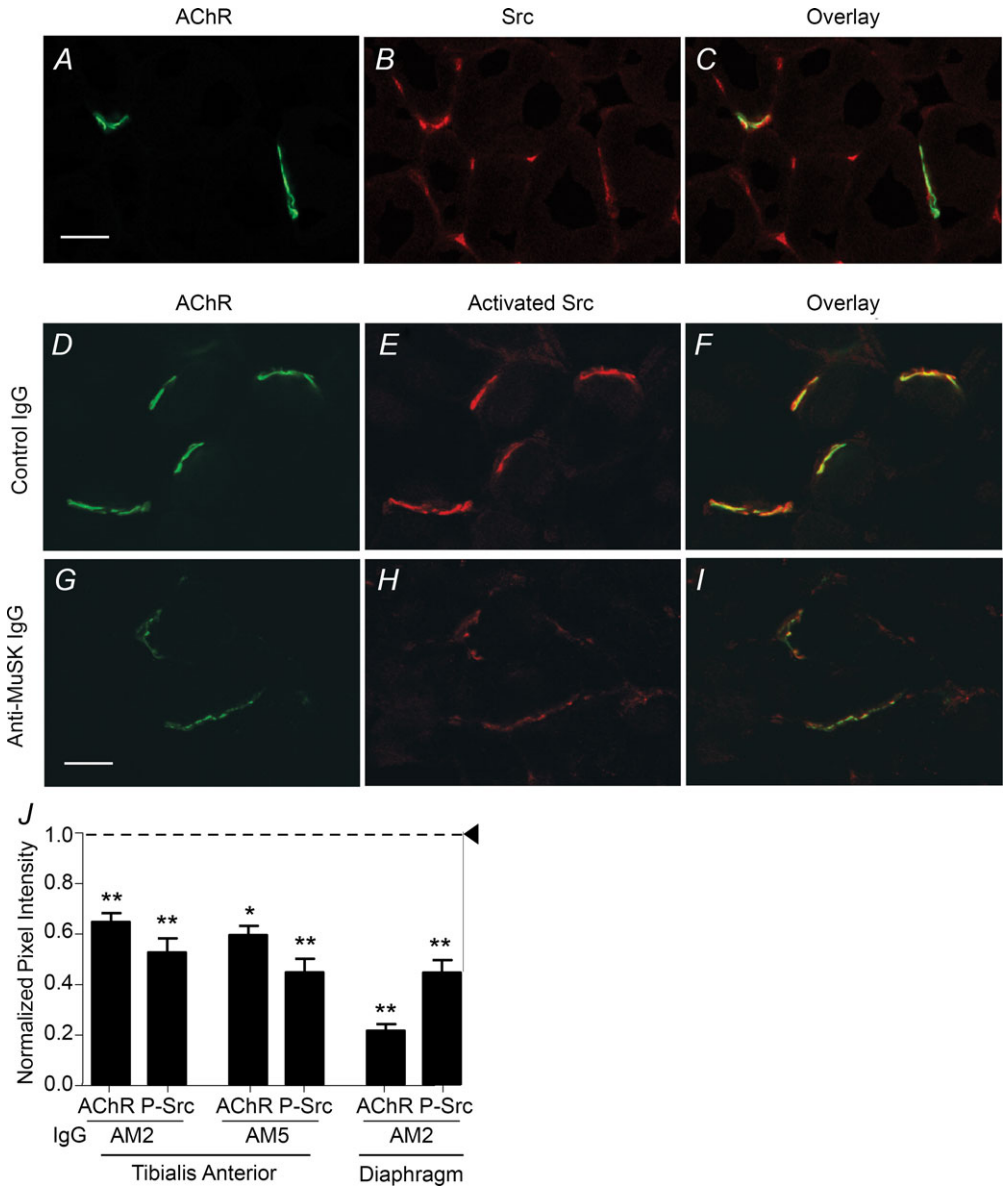

Figure 6. MuSK autoantibodies reduce endplate staining for activated Src
A–C, two healthy endplates from the TA muscle of a control mouse double-labelled for AChR (*A*), total Src (*B*), and the fluorescence overlay (*C*). Immunostaining for total Src was concentrated at endplates but was also at non-synaptic sites on the muscle fibres. *D–F*, four endplates from the TA muscle of a control mouse showing staining for AChR (*D*), activated Src (*E*), and the overlay (*F*). *G–I*, two endplates from the TA muscle of a mouse after 14 daily injections of AM2 IgG showing dim staining for AChR (*G*), activated Src (*H*), and the overlay (*I*). Scale bars in panels *A* and *G* are 20 μm. The brightness and contrast were increased in equal proportion for control and experimental panels for reproduction. *J*, intensity of staining for activated Src and AChR at endplates in the TA and diaphragm muscles of mice after 14 daily injections of AM2 IgG or AM5 IgG. Fluorescence intensity is expressed relative to control mice (horizontal dashed line). Bars represent the mean + SEM for $n = 3$ mice ($^{*}P < 0.05$, $^{**}P < 0.01$ compared to control mice; unpaired Student's *t* test).

pre-existing AChRs during the 6 day test period than mice receiving control IgG. The amount of newly synthesized receptors incorporated into endplates during this period was not significantly less than for control mice. Accelerated loss of pre-existing AChRs from the endplate also occurs after muscle denervation and synaptic blockade, but in such situations there was a compensatory increase in the rate of incorporation of newly synthesized replacement AChRs (Akaaboune *et al.* 1999; Gervásio *et al.* 2007). Based upon the pulse-label data we estimate that the mice injected with AM4.5 IgG suffered a net 40% reduction in the number of endplate AChRs (35% new – 75% removed) over 6 days, which is sufficient to account for previously reported declines in endplate AChR staining in this model of anti-MuSK MG (Fig. 2*L*; Morsch *et al.* 2012). Together, the results suggest that chronic depression of MuSK pathway function at the endplate primarily hampers the retention of AChRs within junctional AChR clusters.

The fate of the AChRs lost from postsynaptic AChR clusters remains uncertain. At healthy NMJs *in vivo* a fraction of the endplate AChRs become internalized into an endosome-like compartment before being returned to the postsynaptic membrane (Bruneau *et al.* 2005). This fraction of recycling AChRs had particularly short half-lives at the endplate (Bruneau & Akaaboune, 2006), suggesting that they tend to be diverted to lysosomal degradation (the eventual fate of AChRs; Hyman & Froehner, 1983; Christianson & Green, 2004). In mice injected with anti-MuSK patient IgG there was an increase

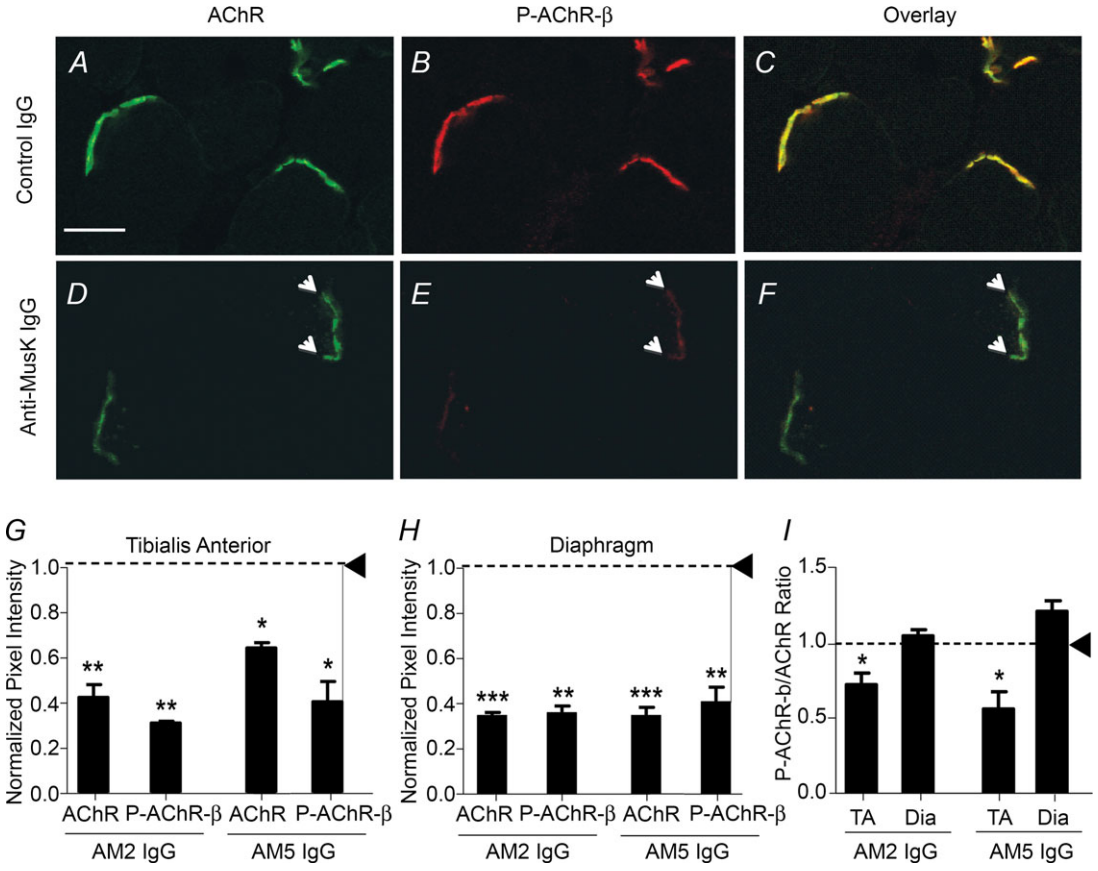

Figure 7. MuSK autoantibodies reduce AChR-β subunit phosphorylation in the TA muscle
A–C, three healthy endplates from the TA muscle of a control mouse double-labelled for total AChR (*A*; Alexa488-α-BGT) and phosphorylated AChR-βY390 (*B*), and the fluorescence overlay (*C*). *D–F*, two endplates from the TA muscle of a mouse after 14 daily injections of AM2 IgG show dim residual staining for total AChR and phospho-AChR-βY390. Arrowheads mark the boundaries of the crescent-shaped AChR staining at one of the endplates. Scale bar in panel *A* is 20 μm. The brightness and contrast were increased in equal proportion for control and experimental panels for reproduction. *G*, intensity of staining for phospho-AChR-βY390 and total AChR at endplates in the TA muscle of mice after 14 daily injections of AM2 IgG or AM5 IgG. Fluorescence intensity is expressed relative to control mice (horizontal dashed line). *H*, comparable results for endplates from the diaphragm muscle. *I*, phospho-AChR-βY390/total-AChR fluorescence intensity ratios for endplates from the TA and diaphragm (Dia) muscles after 14 daily injections of AM2 IgG or AM5 IgG. The horizontal dashed line represents the average for mice injected with control IgG. Bars represent the mean + SEM for $n = 3$ mice ($^*P < 0.05$, $^{**}P < 0.01$, $^{***}P < 0.001$ compared to control mice; unpaired Student's *t* test).

in the proportion of AChRs at the endplate that were not packed into AChR clusters (Cole *et al.* 2010). These stray AChRs could be vulnerable to internalization or might simply diffuse into the extrasynaptic sarcolemma. It is interesting to note that following surface labelling, internalized AChRs could be detected beneath some endplates (Fig. 3*F*).

Recently, Huijbers and others have shown that the dominant IgG4 subclass of anti-MuSK patient antibodies inhibited the assembly of LRP4 with MuSK (Huijbers *et al.* 2013; Koneczny *et al.* 2013). An acute effect of these antibodies was therefore to block agrin-induced MuSK signalling. This finding is not necessarily inconsistent with reduced levels of MuSK at the endplate after several days of anti-MuSK injections. The intensity of endplate staining for MuSK was significantly reduced by four of the six batches of anti-MuSK-positive patient IgG we have so far injected into mice (AM2 and AM3 Cole *et al.* 2010); AM4.5 and AM5 in the present study). The two IgG preparations that did not significantly reduce endplate MuSK staining (AM1 and AM4.1) produced only relatively modest reductions in endplate AChR packing density and the mice showed no weakness (Cole *et al.* 2010). Kawakami *et al.* also reported reduced endplate MuSK staining after 14 daily injections of IgG from one anti-MuSK-positive patient (Kawakami *et al.* 2011). In contrast, mice that were actively immunized with MuSK protein revealed no change in the endplate staining for MuSK (Viegas *et al.* 2012). The mechanism by which MuSK was depleted from the postsynaptic membrane in the passive transfer experiments remains uncertain. Bivalent anti-MuSK IgG can cross-link and activate MuSK (Hopf & Hoch, 1998; Shigemoto *et al.* 2006; Cole *et al.* 2010; Mori *et al.* 2012a,*b*). Activation of MuSK by neural agrin is coupled to MuSK internalization (Lu *et al.* 2007; Zhu *et al.* 2008). When added to cultured heterologous cells, AM2 IgG (2 mg ml^{-1}) also caused MuSK to be internalized (Cole *et al.* 2010). However, anti-MuSK of the dominant IgG4 subclass may be functionally monovalent and not cause MuSK internalization (Huijbers *et al.* 2013; Koneczny *et al.* 2013). Kawakami and colleagues reported that anti-MuSK patient IgG disrupted the binding of MuSK to collagen Q, an interaction that might be important for anchoring MuSK (and collagen Q) at the synaptic cleft (Kawakami *et al.* 2011). Thus it is conceivable that MuSK simply diffuses from the junctional membrane into the adjoining sarcolemma where it might no longer serve the synapse.

The significance of reduced AChR-βY390 phosphorylation remains uncertain. Knock-in mutations in mice that precluded phosphorylation of AChR-βY390 resulted in smaller endplate AChR clusters with slightly looser AChR packing (Friese *et al.* 2007; Borges *et al.* 2008). Thus it is conceivable that the anti-MuSK-induced reduction in AChR-βY390 phosphorylation (Fig. 7) contributed to the accelerated wastage of AChRs from the endplates in the TA muscle. However, this cannot explain the dispersal of endplate AChR clusters that occurred in the diaphragm muscle where there was no change in the phospho-AChR-βY390/total-AChR fluorescence ratio. This muscle-specific difference suggests that regulation of AChR phosphorylation differs between the TA and diaphragm muscles. Some other (unidentified) target of the MuSK pathway may be more critical to maintaining endplate AChR cluster stability.

Reduced endplate AChR staining was a feature of both active immunization and passive IgG transfer models of anti-MuSK MG (Shigemoto *et al.* 2006; Punga *et al.* 2011; Morsch *et al.* 2012). The decline in the total AChR-rich area of the endplate (Morsch *et al.* 2012) could be explained by the loss of large AChR clusters (Fig. 1). In contrast, tiny AChR microaggregates were resistant to the anti-MuSK injections. In the diaphragm muscle AChR microaggregates increased in number and often spread from the endplate into the adjacent sarcolemma (Figs 1 and 3*D*). Rapsyn is involved in forming AChR microaggregates and large AChR clusters, but through different types of interactions. Based upon cryoelectron tomography analysis each AChR pentamer may bind up to three molecules of rapsyn, forming 'struts' that radiate from the AChR channel (Zubera & Unwin, 2013). Self-association of these rapsyn struts appears to draw AChRs together to form microaggregates (Phillips *et al.* 1993; Ramarao & Cohen, 1998; Ramarao *et al.* 2001; Zubera & Unwin, 2013). In contrast, the formation of large, contiguous AChR clusters may depend upon the binding of the carboxyl-terminal RING-H2 domain of rapsyn to β-DG (Apel *et al.* 1995; Bezakova & Bloch, 1998; Cartaud *et al.* 1998; Bartoli *et al.* 2001). Through β-DG, rapsyn may couple AChR microaggregates into a much larger postsynaptic membrane lattice that includes synaptic basement membrane proteins (Sugiyama *et al.* 1997; Montanaro *et al.* 1998; Cote *et al.* 1999; Grady *et al.* 2000; Jacobson *et al.* 2001; Pilgram *et al.* 2010). In mice injected with anti-MuSK patient IgG, β-DG remained resolutely concentrated at the endplate while the intensity of endplate staining for rapsyn and AChR were significantly reduced, suggesting a failure of AChR coupling to the β-DG-rich complex.

The present study suggests that anti-MuSK patient antibodies cause synaptic failure by suppressing signalling in the MuSK pathway of postsynaptic AChR clustering. Repeated daily injections of anti-MuSK patient IgG resulted in reduced intensity of postsynaptic staining for MuSK itself, activated Src, phosphorylated AChR-βY390 and rapsyn. The progressive decline in endplate AChR numbers, reported previously, could be largely explained by impaired retention of AChRs within large endplate AChR clusters. AChRs and rapsyn became dissociated from the β-DG-rich postsynaptic membrane scaffold. The

signalling pathways that regulate the stability of endplate AChR clusters *in vitro* are complex and intertwined. For example protein kinase A interacts with rapsyn to help stabilize postsynaptic AChRs (Röder *et al.* 2010; Choi *et al.* 2012). Neuregulin/ErbB-mediated phosphorylation of α-dystrobrevin is necessary for stabilizing postsynaptic AChRs (Schmidt *et al.* 2011) but neuregulin signalling also potentiates the activation of MuSK (Ngo *et al.* 2012). Further detailed studies will be required to better understand these emerging regulatory networks and precisely how they are affected by MuSK autoantibodies. One caveat concerning passive IgG transfer studies is that (for practical reasons) we can study the effects of IgG from only a few patients. Pathogenic MuSK autoantibodies from different patients may differ in their precise effects upon neuromuscular structure and function, both in mice and in the patients themselves.

References

Akaaboune M, Culican SM, Turney SG & Lichtman JW (1999). Rapid and reversible effects of activity on acetylcholine receptor density at the neuromuscular junction *in vivo*. *Science* **286**, 503–507.

Akaaboune M, Grady RM, Turney S, Sanes JR & Lichtman JW (2002). Neurotransmitter receptor dynamics studied *in vivo* by reversible photo-unbinding of fluorescent ligands. *Neuron* **34**, 865–876.

Apel ED, Roberds SL, Campbell KP & Merlie JP (1995). Rapsyn may function as a link between the acetylcholine receptor and the agrin-binding dystrophin-associated glycoprotein complex. *Neuron* **15**, 115–126.

Ayalon G, Davis JQ, Scotland PB & Bennett V (2008). An ankyrin-based mechanism for functional organization of dytrophin and dystroglycan. *Cell* **135**, 1189–1200.

Bartoli M, Ramarao MK & Cohen JB (2001). Interactions of the rapsyn RING-H2 domain with dystroglycan. *J Biol Chem* **276**, 24911–24917.

Bergamin E, Hallock PT, Burden SJ & Hubbard SR (2010). The cytoplasmic adaptor protein Dok7 activates the receptor tyrosine kinase MuSK via dimerization. *Mol Cell* **39**, 100–109.

Bezakova G & Bloch RJ (1998). The zinc finger domain of the 43-kDa receptor-associated protein, rapsyn: role in acetylcholine receptor clustering. *Mol Cell Neurosci* **11**, 274–288.

Boggon TJ & Eck MJ (2004). Structure and regulation of Src family kinases. *Oncogene* **23**, 7918–7927.

Borges LS & Ferns M (2001). Agrin-induced phosphorylation of the acetylcholine receptor regulates cytoskeletal anchoring and clustering. *J Cell Biol* **153**, 1–11.

Borges LS, Yechikov S, Lee YI, Rudell JB, Friese MB, Burden SJ & Ferns MJ (2008). Identification of a motif in the acetylcholine receptor β subunit whose phosphorylation regulates rapsyn association and postsynaptic receptor localization. *J Neurosci* **28**, 11468–11476.

Bruneau E, Sutter D, Hume RI & Akaaboune M (2005). Identification of nicotinic acetylcholine receptor recycling and its role in maintaining receptor density at the neuromuscular junction *in vivo*. *J Neurosci* **25**, 9949–9959.

Bruneau EG & Akaaboune M (2006). The dynamics of recycled acetylcholine receptors at the neuromuscular junction *in vivo*. *Development* **133**, 4485–4493.

Cartaud A, Coutant S, Petrucci TC & Cartaud J (1998). Evidence for *in situ* and *in vitro* association between β-dystroglycan and the subsynaptic 43K rapsyn protein. *J Biol Chem* **273**, 11321–11326.

Cheng A, Morsch M, Murata Y, Ghazanfari N, Reddel SW & Phillips WD (2013). Sequence of age-associated changes to the mouse neuromuscular junction and the protective effects of voluntary exercise. *PLoS One* **8**, e67970.

Choi KR, Berrera M, Reischl M, Strack S, Albrizio A, Röder IV, Wagner A, Petersen Y, Hafner M, Zaccolo M & Rudolf R (2012). Rapsyn mediates subsynaptic anchoring of PKA type I and stabilisation of acetylcholine receptor *in vivo*. *J Cell Sci* **125**, 714–723.

Christianson JC & Green WN (2004). Regulation of nicotinic receptor expression by the ubiquitin-proteosome system. *EMBO J* **23**, 4156–4165.

Cole RN, Ghazanfari N, Ngo ST, Gervasio OL, Reddel SW & Phillips WD (2010). Patient autoantibodies deplete postsynaptic muscle-specific kinase leading to disassembly of the ACh receptor scaffold and myasthenia gravis in mice. *J Physiol* **588**, 3217–3229.

Cole RN, Reddel SW, Gervásio OL & Phillips WD (2008). Anti-MuSK patient antibodies disrupt the mouse neuromuscular junction. *Ann Neurol* **63**, 782–789.

Cote PD, Moukhles H, Lindenbaum M & Carbonetto S (1999). Chimaeric mice deficient in dystroglycans develop muscular dystrophy and have disrupted myoneural synapses. *Nat Genet* **23**, 338–342.

Drummond GB (2009). Reporting ethical matters in *The Journal of Physiology*: standards and advice. *J Physiol* **587**, 713–719.

Finn AJ, Feng G & Pendergast AM (2003). Postsynaptic requirements for Abl kinases in assembly of the neuromuscular junction. *Nat Neurosci* **6**, 717–723.

Friese MB, Blagden CS & Burden SJ (2007). Synaptic differentiation is defective in mice lacking acetylcholine receptor β-subunit tyrosine phosphorylation. *Development* **134**, 4167–4176.

Fuhrer C, Gautam M, Sugiyama JE & Hall ZW (1999). Roles of rapsyn and agrin in interaction of postsynaptic proteins with acetylcholine receptors. *J Neurosci* **19**, 6405–6416.

Fuhrer C & Hall ZW (1996). Functional interaction of Src family kinases with the acetylcholine receptor in C2 myotubes. *J Biol Chem* **271**, 32474–32481.

Gautam M, Noakes PG, Mudd J, Nichol M, Chu GC, Sanes JR & Merlie JP (1995). Failure of postsynaptic specialization to develop at neuromuscular junctions of rapsyn deficient mice. *Nature* **377**, 232–236.

Gervásio OL, Armson PF & Phillips WD (2007). Developmental increase in the amount of rapsyn per acetylcholine receptor promotes postsynaptic receptor packing and stability. *Dev Biol* **305**, 262–275.

Gervásio OL & Phillips WD (2005). Increased ratio of rapsyn to ACh receptor stabilizes postsynaptic receptors at the mouse neuromuscular synapse. *J Physiol* **562**, 673–685.

Glass DJ, Bowen DC, Stitt TN, Radiejewski C, Brunno J, Ryan TE, Gies DR, Shah S, Mattsson K, Burden SJ, DiStefano PS, Valenzuela DM, DeChiara TM & Yancopoulos GD (1996). Agrin acts via a MuSK receptor complex. *Cell* **85**, 513–523.

Grady RM, Zhou H, Cunningham JM, Henry MD, Campbell KP & Sanes JR (2000). Maturation and maintenance of the neuromuscular synapse: genetic evidence for roles of the dystrophin-glycoprotein complex. *Neuron* **25**, 279–293.

Higuchi O, Hamuro J, Motomura M & Yamanashi Y (2011). Autoantibodies to low-density lipoprotein receptor-related protein 4 in myasthenia gravis. *Ann Neurol* **69**, 418–422.

Hoch W, McConville J, Helms S, Newsom-Davis J, Melms A & Vincent A (2001). Autoantibodies to the receptor tyrosine kinase MuSK in patients with myasthenia gravis without acetylcholine receptor antibodies. *Nat Med* **7**, 365–368.

Hopf C & Hoch W (1998). Dimerization of the muscle-specific kinase induces tyrosine phosphorylation of acetylcholine receptors and their aggregation on the surface of myotubes. *J Biol Chem* **273**, 6467–6473.

Huebsch KA & Maimone MM (2003). Rapsyn-mediated clustering of acetylcholine receptor subunits requires the major cytoplasmic loop of the receptor subunits. *J Neurobiol* **54**, 486–501.

Huijbers MG, Zhang W, Klooster R, Niks EH, Friese MB, Straasheijm IR, Thijssen PE, Vrolijk H, Plomp JJ, Vogels P, Losen M, van der Maarel SM, Burden SJ & Verschuuren JJ (2013). MuSK IgG4 auto-antibodies cause myasthenia gravis by inhibiting binding between MuSK and Lrp4. *Proc Natl Acad Sci U S A* **110**, 20783–20788.

Hyman C & Froehner SC (1983). Degradation of acteylcholine receptors in muscle cells: effect of leupeptin on turnover rate, intracellular pool sizes, and receptor properties. *J Cell Biol* **95**, 1316–1324.

Jacobson C, Cote PD, Rossi SG, Rotundo RL & Carbonetto S (2001). The dystroglycan complex is necessary for stabilization of acetylcholine receptor clusters at neuromuscular junctions and formation of the synaptic basement membrane. *J Cell Biol* **152**, 435–450.

Kahl J & Campanelli JT (2003). A role for the juxtamembrane domain of β-dystroglycan in agrin-induced acetylcholine receptor clustering. *J Neurosci* **23**, 392–402.

Kawakami Y, Ito M, Hirayama M, Sahashi K, Ohkawara B, Masuda A, Nishida H, Mabuchi N, Engel AG & Ohno K (2011). Anti-MuSK autoantibodies block binding of collagen Q to MuSK. *Neurology* **77**, 1–8.

Kim N & Burden SJ (2008). MuSK controls where motor axons grow and form synapses. *Nat Neurosci* **11**, 19–27.

Kim N, Stiegler AL, Cameron TO, Hallock PT, Gomez AM, Huang JH, Hubbard SR, Dustin ML & Burden SJ (2008). Lrp4 is a receptor for agrin and forms a complex with MuSK. *Cell* **135**, 334–342.

Klooster R, Plomp JJ, Huijbers MG, Niks EH, Straasheijm KR, Detmers FJ, Hermans PW, Sleijpen K, Verrips A, Losen M, Martinex-Martinez P, De Baets MH, van der Maarel S & Verschuuren JJ (2012). Muscle-specific kinase myasthenia gravis IgG4 autoantibodies cause severe neuromuscular junction dysfunction in mice. *Brain* **135**, 1081–1101.

Koneczny I, Cossins J, Waters P, Beeson D & Vincent A (2013). MuSK myasthenia gravis IgG4 disrupts the interaction of LRP4 with MuSK but both IgG4 and IgG1-3 can disperse preformed agrin-Independent AChR clusters. *PLoS One* **11**, e80695.

le Coutre P, Mologni L, Cleris L, Marchesi E, Buchdunger E, Giardini R, Formelli F & Gamacorti-Passerini C (1999). In vivo eradication of human BCR/ABL-positive leukemia cells with an ABL kinase inhibitor. *J Natl Cancer Inst* **91**, 163–168.

Lee Y, Rudell J & Ferns M (2009). Rapsyn interacts with the muscle acetylcholine receptor via α-helical domains in the α, β, and ε subunit intracellular loops. *Neuroscience* **163**, 222–232.

Lefebvre JL, Juing L, Becaficco S, Franzini-Armstrong C & Granato M (2007). Differential requirement for MuSK and dystroglycan in generating patterns of neuromuscular innervation. *Proc Natl Acad Sci U S A* **104**, 2483–2488.

Losen M, Stassen MHW, Martinez-Martinez P, Machiels B, Duimel H, Frederik P, Veldman H, Wokke JHJ, Spaans F, Vincent A & DeBaets M (2005). Increased expression of rapsyn in muscles prevents acetylcholine receptor loss in experimental autoimmune myasthenia gravis. *Brain* **128**, 2327–2337.

Lu Z, Je H-S, Young P, Gross J, Lu B & Feng G (2007). Regulation of synaptic growth and maturation by a synapse-associated E3 ubiquitin ligase at the neuromuscular junction. *J Cell Biol* **177**, 1077–1089.

McConville J, Farrugia ME, Beeson D, Kishore U, Metcalf R, Newsom-Davis J & Vincent A (2004). Detection and characterization of MuSK antibodies in seronegative myasthenia gravis. *Ann Neurol* **55**, 580–584.

McMahan UJ & Slater CR (1984). The influence of basal lamina on the accumulation of acetylcholine receptors at synaptic sites in regenerating muscle. *J Cell Biol* **98**, 1453–1473.

Mittaud P, Camilleri AA, Willmann R, Ern-Vogtli S, Burden SJ & Fuhrer C (2004). A single pulse of agrin triggers a pathway that acts to cluster acetylcholine receptors. *Mol Cell Biol* **24**, 7841–7854.

Mittaud P, Marangi PA, Erb-Vogtli S & Fuhrer C (2001). Agrin-activation of acetylcholine receptor-bound src family kinases requires rapsyn and correlates with acetylcholine receptor clustering. *J Biol Chem* **276**, 14505–14513.

Mohamed AS, Rivas-Plata KA, Kraas JR, Saleh SM & Swope SL (2001). Src-class kinases act within the agrin/MuSK pathway to regulate acetylcholine receptor phosphorylation, cytoskeletal anchoring, and clustering. *J Neurosci* **21**, 3806–3818.

Montanaro F, Gee SH, Jacobson C, Lindenbaum MH, Froehner SC & Carbonetto S (1998). Laminin and α-dystroglycan mediate acetylcholine receptor aggregation via a MuSK-independent pathway. *J Neurosci* **18**, 1250–1260.

Moransard M, Borges LS, Willmann R, Marangi PA, Brenner HR, Ferns MJ & Fuhrer C (2003). Agrin regulates rapsyn interaction with surface AChRs which underlies cytoskeletal anchoring and clustering. *J Biol Chem* **278**, 7350–7359.

Mori S, Kubo S, Akiyoshi T, Yamada S, Miyazaki T, Hotta H, Desaki J, Kishi M, Konishi T, Nishino Y, Miyazawa A, Maruyama N & Shigemoto K (2012a). Antibodies against muscle-specific kinase impair both presynaptic and postsynaptic functions in a murine model of myasthenia gravis. *Am J Pathol* **180**, 798–810.

Mori S, Yamada S, Kubo S, Chen J, Matsuda S, Shudou M, Maruyama N & Shigemoto K (2012b). Divalent and monovalent autoantibodies cause dysfunction of MuSK by distinct mechanisms in a rabbit model of myasthenia gravis. *J Neuroimmunol* **244**, 1–7.

Morsch M, Reddel SW, Ghazanfari N, Toyka KV & Phillips WD (2012). Muscle specific kinase autoantibodies cause synaptic failure through progressive wastage of postsynaptic acetylcholine receptors. *Exp Neurol* **237**, 286–295.

Morsch M, Reddel SW, Ghazanfari N, Toyka KV & Phillips WD (2013). Pyridostigmine but not 3,4-diaminopyridine exacerbates ACh receptor loss and myasthenia induced in mice by muscle-specific kinase autoantibody. *J Physiol* **591**, 2747–2762.

Ngo ST, Cole RN, Sunn N, Phillips WD & Noakes PG (2012). Neuregulin-1 potentiates agrin-induced acetylcholine receptor clustering via muscle-specific kinase phosphorylation. *J Cell Sci* **125**, 1531–1543.

Niks EH, Kuks JBM, Wokke JHJ, Veldman H, Bakker E, Verschuuren JJGM & Plomp JJ (2010). Pre- and postsynaptic neuromuscular junction abnormalities in MuSK myasthenia. *Muscle Nerve* **42**, 283–288.

Ohno K, Ito M, Kawakami Y & Ohtsuka K (2013). Collagen Q is a key player for developing rational therapy for congenital myasthenia and for dissecting the mechanisms of anti-MuSK myasthenia gravis. *J Mol Neurosci* DOI: 10.1007/s12031-013-0170-x.

Ohta K, Shigemoto K, Fujinami A, Maruyama N, Konishi T & Ohta M (2007). Clinical and experimental features of MuSK antibody positive MG in Japan. *Eur J Neurol* **14**, 1029–1034.

Peng HB & Froehner SC (1985). Association of the postsynaptic 43K protein with newly formed acetylcholine receptor clusters in cultured muscle cells. *J Cell Biol* **100**, 1698–1705.

Pevzner A, Schoser B, Peters K, Cosma NC, Karakatsani A, Schalke B, Melms A & Kröger S (2011). Anti-LRP4 autoantibodies in AChR- and MuSK-antibody-negative myasthenia gravis. *J Neurol* **259**, 427–435.

Phillips WD, Noakes PG, Roberds SL, Campbell KP & Merlie JP (1993). Clustering and immobilization of acetylcholine receptors by the 43-kD protein: a role for dystrophin-related protein. *J Cell Biol* **123**, 729–740.

Pilgram GSK, Potikanond S, Baines RA, Fradkin LG & Noordermeer JN (2010). The roles of the dystrophin-associated glycoprotein complex at the synapse. *Mol Neurobiol* **41**, 1–21.

Pumplin DW & Bloch RJ (1987). Disruption and reformation of the acetylcholine receptor clusters of cultured rat myotubes occur in two distinct stages. *J Cell Biol* **104**, 97–108.

Punga AR, Lin S, Oliveri F, Meinen S & Ruegg MA (2011). Muscle-selective synaptic disassembly and reorganization in MuSK antibody-positive MG mice. *Exp Neurol* **230**, 207–217.

Ramarao MK, Bianchetta MJ, Lanken J & Cohen JB (2001). Role of rapsyn tetratrico repeat and coiled-coil domains in self association and nicotinic acetylcholine receptor clustering. *J Biol Chem* **276**, 7475–7483.

Ramarao MK & Cohen JB (1998). Mechanism of nicotinic acetylcholine receptor cluster formation by rapsyn. *Proc Natl Acad Sci U S A* **95**, 4007–4012.

Richman DP, Nishi K, Morell SW, Chang JM, Ferns MJ, Wollmann RL, Maselli RA, Schnier J & Agius MA (2011). Acute severe animal model of anti-muscle-specific kinase myasthenia. *Arch Neurol* **69**, 453–460.

Röder IV, Choi K-R, Reischl M, Petersen Y, Diefenbacher ME, Zaccolo M, Pozzan T & Rudolf R (2010). Myosin Va cooperates with PKA RIα to mediate maintenance of the endplate *in vivo*. *Proc Natl Acad Sci U S A* **107**, 2031–2036.

Sadasivam G, Willman R, Lin S, Erb-Vogtli S, Kong XC, Ruegg MA & Fuhrer C (2005). Src-family kinases stabilize the neuromuscular synapse via protein interactions, phosphorylation, and cytoskeletal linkage. *J Neurosci* **25**, 10479–10493. .

Schmidt N, Akaaboune M, Gajendran N, Martinez-Pena Y, Valenzuela I, Wakefield S, Thurnheer R & Brenner HR (2011). Neuregulin/ErbB regulate neuromuscular junction development by phosphorylation of α-dystrobrevin. *J Cell Biol* **195**, 1171–1184.

Selcen D, Fukuda T, Shen X-M & Engel AG (2004). Are MuSK antibodies the primary cause of myasthenic symptoms? *Neurology* **62**, 1945–1950.

Shen C, Lu Y, Zhang B, Figueiredo D, Bean J, Jung J, Wu H, Barik A, Yin D-M, Xiong W-C & Mei L (2013). Antibodies against low-density lipoprotein receptor-related protein 4 induce myasthenia gravis. *J Clin Invest* 123, 5190–5202.

Shigemoto K, Kubo S, Maruyama N, Hato N, Yamada H, Jie C, Kobayashi N, Mominoki K, Abe Y, Ueda N & Matsuda S (2006). Induction of myasthenia by immunization against muscle-specific kinase. *J Clin Invest* **116**, 1016–1024.

Shiraishi H, Motomura M, Yoshimura T, Fukudome T, Fukuda T, Nakao Y, Tsujihata M, Vincent A & Eguchi K (2005). Acetylcholine receptors loss and postsynaptic damage in MuSK antibody-positive myasthenia gravis. *Ann Neurol* **57**, 289–293.

Stacy S, Gelb BE, Koop BA, Windle JJ, Wall KA, Krolick KA, Infante AJ & Kraig E (2002). Split tolerance in a novel transgenic model of autoimmune myasthenia gravis. *J Immunol* **169**, 6570–6579.

Sugiyama JE, Glass DJ, Yancopoulos GD & Hall ZW (1997). Laminin-induced acetylcholine receptor clustering: an alternative pathway. *J Cell Biol* **139**, 181–191.

Toyka KV, Drachman DB, Griffin DE, Pestronk A, Winkelstein JA, Fishbeck KH & Kao I (1977). Myasthenia gravis. Study of humoral immune mechanisms by passive transfer to mice. *N Engl J Med* **296**, 125–131.

Viegas S, Jacobson L, Waters P, Cossins J, Jacob S, Leite MI, Webster R & Vincent A (2012). Passive and active immunization models of MuSK-Ab positive myasthenia: Electrophysiological evidence for pre and postsynaptic defects. *Exp Neurol* **234**, 506–512.

Weston C, Gordon C, Teressa G, Hod E, Ren X-D & Prives J (2003). Cooperative regulation by Rac and Rho of agrin-induced acetylcholine receptor clustering in muscle cells. *J Biol Chem* **278**, 6450–6455.

Zhang B, Luo S, Wang Q, Suzuki T, Xiong WC & Mei L (2008). LRP4 serves as a coreceptor of agrin. *Neuron* **60**, 285–297.

Zhu D, Yang Z, Luo Z, Luo S, Xiong WC & Mei L (2008). Muscle-specific receptor tyrosine kinase endocytosis in acetylcholine receptor clustering in response to agrin. *J Neurosci* **28**, 1688–1696.

Zubera B & Unwin N (2013). Structure and superorganization of acetylcholine receptor–rapsyn complexes. *Proc Natl Acad Sci U S A* **110**, 10622–10627.

Additional information

Competing interests

The authors have no competing interests.

Author contributions

N.G., M.M., S.W.R., S.X.L. and W.D.P. contributed to the conception and design of the experiments. All of the experiments were performed at Physiology, University of Sydney by N.G. and M.M. All authors contributed to the drafting and revision of the article, and approved the final version of the manuscript.

Funding

This work was supported by the National Health and Medical Research Council (570930 to W.D.P and S.W.R.), the Brain Foundation, The Beeren Foundation, and the Australian Myasthenic Association in New South Wales.

Acknowledgements

We thank Dr Louise Cole and the Bosch Institute Advanced Imaging Facility for technical advice and support. We also thank the apheresis team, Sr Beth Newman, the molecular medicine laboratory at Concord Hospital, Louise Wienholt and patients from around Australia who contributed their plasma to this research.

Translational perspective

Myasthenia gravis (MG) is a muscle weakness disease caused by autoantibodies that disrupt synaptic transmission at the neuromuscular junction. Muscle-specific kinase (MuSK) is a receptor tyrosine kinase important for stabilizing the developing neuromuscular junction. Approximately 10% of MG patients are seropositive for MuSK autoantibodies. In previous studies, mice injected with IgG from anti-MuSK MG patients reproduced pathophysiological symptoms of anti-MuSK MG. In particular, synaptic transmission at the neuromuscular junction was hindered. Here we show when IgG from anti-MuSK patients was injected into mice it suppressed the levels of several components of the MuSK signalling pathway at the neuromuscular junction. This suggests that MuSK autoantibodies cause failure of neuromuscular synaptic transmission by interrupting physiological tyrosine kinase signalling at the synapse that relies upon MuSK. Some caution is required in translating these findings because anti-MuSK autoantibodies from individual patients might vary in precisely how they interact with MuSK and cause disease. Moreover there are insufficient human biopsy studies at present to know whether anti-MuSK MG in humans involves the same molecular changes as those found in rodent models of the disease.